Constraining the source separation with coda wave interferometry: Theory and application to earthquake doublets in the Hayward fault, California

Roel Snieder and Mark Vrijlandt

Department of Geophysics and Center for Wave Phenomena, Colorado School of Mines, Golden, Colorado, USA

Received 12 July 2004; revised 22 December 2004; accepted 14 January 2005; published 2 April 2005.

[1] The relative location of seismic sources is of importance for the location of aftershocks on a fault, for the positioning of sources in repeat seismic surveys, and for monitoring induced seismicity. In this paper we show how the seismic coda can be used to infer a measure of the source separation of two identical seismic sources from the correlation of the waveforms recorded at a single receiver. The theory is applicable to an explosive source in an acoustic or elastic medium and for a point force or double couple in an elastic medium. For an explosive source the source separation is constrained to be located on a sphere, while for a point force and a double couple the source separation can be constrained to be located on an ellipsoid whose symmetry axis is determined by the point force or double couple. We validate the theory with synthetic seismograms and apply the theory to earthquake doublets on the Hayward fault, California. The distance between events obtained from the coda waves agrees with the distance obtained from the double-difference method.

Citation: Snieder, R., and M. Vrijlandt (2005), Constraining the source separation with coda wave interferometry: Theory and application to earthquake doublets in the Hayward fault, California, *J. Geophys. Res.*, *110*, B04301, doi:10.1029/2004JB003317.

1. Introduction

[2] In a number of applications it is useful to determine the relative location of seismic sources. Aftershocks after a large earthquake help constrain the location and extent of the fault plane [*Lay and Wallace*, 1995]. Earthquake clusters have been used to locate fault planes, both in a tectonic setting [e.g., *Fuis et al.*, 2001] and in hydrocarbon reservoirs [*Maxwell and Urbancic*, 2001]. Seismicity can be used to monitor the fluid transport properties in reservoirs [*Shapiro et al.*, 2002]. In repeat seismic surveys with down hole sources, it is essential that the source separation in the two surveys is known with great accuracy in order to reduce the imprint of errors in the source location in time lapse measurements.

[3] In principle, the relative position of two source locations can be found by locating each of the sources, and subsequently computing their relative location. The disadvantage of this approach is that errors in the velocity model along the whole path from the sources to the receivers may erroneously be mapped into location errors. The relative position computed by comparing the absolute locations may be dominated by the location errors for the individual sources [*Pavlis*, 1992]. For this reason it is advantageous to determine the source separation directly from the recorded waveforms.

[4] Earthquakes that occur within the same cluster of events often generate waveforms that are highly repeatable. Such highly repeatable waveforms have been used to constrain the relative positions of these by measuring the delay times between the arriving P and S waves of the different events [*Poupinet et al.*, 1984; *Frémont and Malone*, 1987; *Got et al.*, 1994; *Nadeau and McEvilly*, 1997; *Bokelmann and Harhes*, 2000; *Waldhauser and Ellsworth*, 2000]. Such a measurement of the delay time of P and S waves has also been used to find the relative location between one master event and a number of smaller events [*Ito*, 1985; *Scherbaum and Wendler*, 1986; *Frémont and Malone*, 1987; *VanDecar and Crosson*, 1990; *Deichmann and Garcia-Fernandez*, 1992; *Lees*, 1998]. Usually, this delay time is measured by a cross correlation of the direct P and S arrivals for the different events. A robust variation of this idea is based on a measurement of the cross correlation of the direct P and S waves that is based on an L_1 norm and a nearest-neighbor approach [*Shearer*, 1997; *Astiz and Shearer*, 2000].

[5] In this paper we propose a technique to obtain a measure of the relative source location of two events that is based on coda waves. The main idea is that the energy that constitutes the coda waves is radiated in all directions with a radiation pattern that is determined by the source mechanism. When the source position changes, some wave paths will be longer while other wave paths become shorter. This is illustrated in Figure 1 where the original and perturbed source locations are indicated with solid and open circles, respectively. The wave paths from the original source position and perturbed source position to the first scatterer along each trajectory are shown with solid and dashed lines, respectively. Some trajectories are longer due to the source

0148-0227/05/2004JB003317$09.00

displacement while others are shorter. This changes the interference pattern of the scattered waves that constitute the coda. Here we use the change in the coda waves to constrain the relative locations of the events. This technique is a new application of coda wave interferometry [*Snieder et al.*, 2002; *Snieder*, 2002, 2004b].

[6] When the source position changes, only the path length to the first scatterer along each trajectory changes; the later parts of the trajectories is unchanged. In single scattering the waves travel from the first scatterer directly to the receiver, while in multiple scattering the waves first travel to other scatterers before reaching the receiver. The later part of the trajectories are unchanged under a perturbation in the source location, therefore the technique presented here is valid both for single scattering as well as for multiple scattering.

[7] The principles of coda wave interferometry are introduced in section 2. The displacement of an isotropic source in an acoustic medium is treated in section 3. The generalization to an elastic medium that is excited by a point force and of a double couple is presented in sections 4 and 5.1. The source displacement of an explosive source in an elastic medium is treated in section 5.2. The application of the theory is discussed in section 6. The theory is validated with synthetic seismograms (section 7). We show the application of the theory to earthquake doublets on the Hayward fault, California, in section 8.

2. Coda Wave Interferometry and Source Displacement

[8] In this section, we review the elements of coda wave interferometry. A more detailed description is given by *Snieder* [2002]. The idea of coda wave interferometry is based on path summation [*Snieder*, 1999]. In this approach the wave field is written as a superposition of the waves that follow all the different scattering paths in the medium:

$$\mathbf{u}^{(u)}(t) = \sum_T \mathbf{A}_T(t) \; . \tag{1}$$

The subscript T labels the different trajectories along which the waves have traveled. A trajectory not only specifies the path that a wave has taken through space, it also specifies which of the segments along that path have been traversed as a P wave or as an S wave. The summation over trajectories therefore also contains a summation over the different wave modes (P or S) that an elastic wave can take while propagating between the scatterers along each path. The function $\mathbf{A}_T(t)$ denotes the contribution of the trajectory T to the waveform recorded at the station under consideration. The superscript (u) in equation (1) denotes that this is the unperturbed waveform, i.e., that associated with the reference source position.

[9] Suppose that the source location is perturbed but that the source mechanism is unchanged. A change in the source location changes for each trajectory the arrival time of the wave, the geometrical spreading for the propagation to the first scatterer, and for a nonisotropic source and for nonisotropic scattering, the amplitude of the wave. We show in Appendix A that the change in the waves due to a change in the arrival time is larger to the other changes by a factor $l/m\lambda$, where l is the mean free path, λ the dominant wavelength, and m the order of the Fourier expansion of the radiation pattern of the source or the scattering amplitude. (Usually, $|m| \leq 2$.) Coda waves usually show distinct P and S wave arrivals, they are therefore not localized and $l \gg \lambda$ [*van Tiggelen*, 1999]. The dominant change to the wave field thus comes from the travel time perturbation τ_T for the wave along each trajectory T, and the perturbed wave field is given by

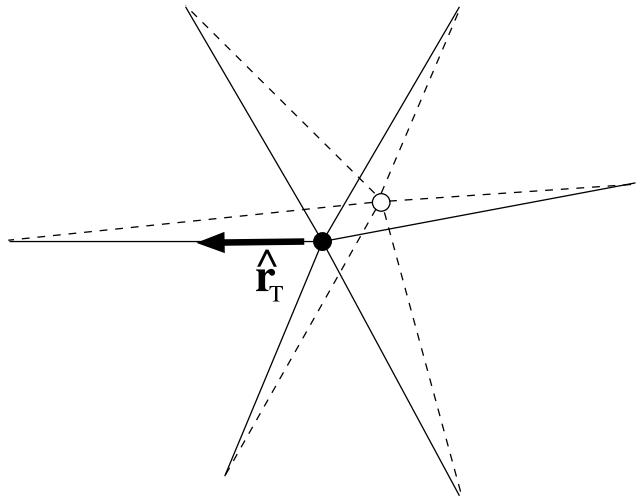

Figure 1. Unperturbed source position (solid circle) and perturbed source position (open circle). The path from the unperturbed source to the first scatterer along each path is indicated with solid lines. The corresponding path for the perturbed source position is shown by dashed lines.

$$\mathbf{u}^{(p)}(t) = \sum_T \mathbf{A}_T(t - \tau_T) \; . \tag{2}$$

Note that we do not assume that the scattering is isotropic.

[10] The change in the waveform can be measured by a time-shifted cross correlation, with shift time t_s computed over a time window of length $2t_w$ and center time t:

$$R^{(t,t_w)}(t_s) \equiv \frac{\int_{t-t_w}^{t+t_w} u_i^{(u)}(t') u_i^{(p)}(t'+t_s) dt'}{\left(\int_{t-t_w}^{t+t_w} u_i^{(u)2}(t') dt' \int_{t-t_w}^{t+t_w} u_i^{(p)2}(t') dt' \right)^{1/2}} \; . \tag{3}$$

As shown by *Snieder* [2002], this cross correlation attains its maximum value for

$$t_s = \langle \tau \rangle_{(t,t_w)} \; , \tag{4}$$

where the average in expression (4) is given by

$$\langle \tau \rangle_{(t,t_w)} = \frac{\sum_T A_T^2 \tau_T}{\sum_T A_T^2} \; . \tag{5}$$

In expression (5) the summation is over the trajectories with an arrival time within the interval $(t - t_w, t + t_w)$. The maximum value of the cross correlation is given by [*Snieder*, 2002]

$$R_{\max}^{(t,t_w)} = 1 - \frac{1}{2} \overline{\omega^2} \sigma_\tau^2 \; , \tag{6}$$

where σ_τ is the variance of the travel time perturbation defined as

$$\sigma_\tau^2 = \frac{\sum_T A_T^2 (\tau_T - \langle\tau\rangle)^2}{\sum_T A_T^2} , \quad (7)$$

where the sum is over all trajectories with an arrival time in the employed time window. The frequency $\overline{\omega^2}$ is given by

$$\overline{\omega^2} \equiv -\frac{\int_{t-t_w}^{t+t_w} u^{(u)}(t')\ddot{u}^{(u)}(t')dt'}{\int_{t-t_w}^{t+t_w} u^{(u)2}(t')dt'} = \frac{\int_{t-t_w}^{t+t_w} \dot{u}^{(u)2}(t')dt'}{\int_{t-t_w}^{t+t_w} u^{(u)2}(t')dt'} . \quad (8)$$

The cross correlation R decreases for increasing values of σ_τ^2. With increasing values of σ_τ^2, the relative arrival times of the scattered waves are perturbed, which leads to a change in the interfering scattered waves that constitute the coda. This is reflected by a decreasing value of the cross correlation R.

[11] This theory is based on two approximations [*Snieder*, 2002]. When the expressions (1) and (2) are inserted in the cross correlation, a double sum $\sum_{TT'}$ over trajectories results. This double sum can be decomposed into diagonal terms and cross terms: $\sum_{TT'} = \sum_{T=T'} + \sum_{T\neq T'}$. In coda wave interferometry these cross terms are neglected [*Snieder*, 2002]. The second approximation is that expression (6) is based on a second-order Taylor expansion of the cross correlation in the quantity $\tau_T - \langle\tau\rangle$ [*Snieder*, 2002]. This approximation is valid when this time is small compared to the width of the cross correlation. This condition is satisfied when $\overline{\omega}\sigma_\tau$ is smaller than one. Physically, this means that the theory is valid when the shift in the arrival time due to the source perturbation is smaller than a period. The perturbation in the source location therefore must be smaller than a wavelength.

[12] The cross correlation (3) can readily be computed given the measured unperturbed and the perturbed waveforms, so both the location and the peak value of the normalized cross correlation can be measured. With expressions (4) and (6) the mean and variance of the travel time perturbations can therefore be determined from the observations.

[13] When the source location is perturbed, only the length of the wave path to the first scatterer along each path is perturbed, because a perturbation in the source location does not change the relative positions of the scatterers along a path. The travel time change due to a perturbation δ in the source location leads to a change in the travel time for the wave that travels along trajectory T that is given by

$$\tau_T = -\frac{1}{v}(\hat{\mathbf{r}}_T \cdot \delta) . \quad (9)$$

As shown in Figure 1, the unit vector $\hat{\mathbf{r}}_T$ points in the direction in which the trajectory T takes off at the source. In the last expression the velocity v is the velocity of the trajectory as it leaves the source, this can either be the P velocity or the S velocity. We assume throughout this paper that the velocity is constant over the region over which the source is displaced and that the velocity is isotropic.

[14] When the scatterers are distributed homogeneously, the summation over all trajectories that leave the source can be replaced by an angular integration over all directions with which a wave can leave the source. Since the averages (5) and (7) are taken with a weight given by the energy of the wave that travels along each the trajectory, the integration over all takeoff directions at the source is to be weighted with the radiated energy in those directions. This principle is used in this work to compute the mean and variance of the travel time caused by changes in the source location.

3. An Isotropic Source in an Acoustic Medium

[15] In this section we consider the simplest case of a displacement of an isotropic source in an acoustic medium. We assume that the propagation of the waves from the source to the first scatterer along each path can be described by the Green's function for a homogeneous medium. For an isotropic source at the origin with source spectrum $S(\omega)$, the waves that propagate to the first scatterer along each path are thus given by

$$u(r) = -\frac{e^{ikr}}{4\pi r} S(\omega) . \quad (10)$$

[16] When the scatterers in the medium are distributed homogeneously, the travel time perturbation due to a source displacement δ for each trajectory is given by (9) and the mean travel time perturbation (5) is given by

$$\langle\tau\rangle = \frac{-\int\int \left|-\frac{e^{ikr}}{4\pi r}\right|^2 \frac{1}{v}(\hat{\mathbf{r}}\cdot\delta)|S(\omega)|^2 d\Omega d\omega}{\int\int \left|-\frac{e^{ikr}}{4\pi r}\right|^2 |S(\omega)|^2 d\Omega d\omega} , \quad (11)$$

where $\int\cdots d\Omega$ denotes the angular integration over all outgoing directions, $\int\cdots d\omega$ denotes an integration over frequency, and r is the distance to the first scatterer in each direction. When the scatterers are distributed homogeneously, this distance is on average the same for each direction, and expression (11) can be rewritten as

$$\langle\tau\rangle = \frac{-\int(\hat{\mathbf{r}}\cdot\delta)d\Omega \int|S(\omega)|^2 d\omega}{4\pi v \int|S(\omega)|^2 d\omega} . \quad (12)$$

The frequency integrals cancel so that

$$\langle\tau\rangle = -\frac{1}{4\pi v}\int(\hat{\mathbf{r}}\cdot\delta)d\Omega . \quad (13)$$

The integrand is an odd function of the location $\hat{\mathbf{r}}$ on the unit sphere. Since we integrate over the full unit sphere this integral vanishes:

$$\langle\tau\rangle = 0 . \quad (14)$$

Physically this reflects the fact that as the source location is moved, some paths become longer, while others become shorter, see Figure 1. On average, the associated imprint on the travel time is zero.

[17] Since the mean travel time perturbation vanishes, $\sigma_\tau^2 = \langle\tau^2\rangle - \langle\tau\rangle^2 = \langle\tau^2\rangle$. This quantity can be computed

using the same reasoning that led to (13), the only difference being that $\tau = -v^{-1}(\hat{\mathbf{r}}\cdot\delta)$ needs to be replaced by $\tau^2 = v^{-2}(\hat{\mathbf{r}}\cdot\delta)^2$, this gives

$$\sigma_\tau^2 = \frac{1}{4\pi v^2}\int(\hat{\mathbf{r}}\cdot\delta)^2 d\Omega\,. \tag{15}$$

Expression (15) is most easily evaluated by using

$$\hat{\mathbf{r}} = \begin{pmatrix}\cos\varphi\sin\theta\\ \sin\varphi\sin\theta\\ \cos\theta\end{pmatrix}, \tag{16}$$

with θ and φ the colatitude and longitude used in a system of spherical coordinates. Aligning the z axis of the integration variable with the source displacement δ reduces the angular integral in (15) to $\delta^2\int\cos^2\theta d\Omega = 4\pi\delta^2/3$, and hence

$$\sigma_\tau^2 = \frac{1}{3}\frac{\delta^2}{v^2}\,. \tag{17}$$

[18] Using coda wave interferometry, we can use equation (6) to infer σ_τ^2 from the changes in the waveform. Then, from (17), we can infer the magnitude δ of the source displacement, but not the direction of the source displacement. Expression (17) was used by *Snieder and Hagerty* [2004] to estimate the temporal change in the point of excitation of volcanic tremors in Arenal Volcano, Costa Rica.

[19] The change in the arrival time of the first arriving wave constrains $(\hat{\mathbf{t}}\cdot\delta)$, with $\hat{\mathbf{t}}$ the unit vector in the takeoff direction of a ray at the source that propagates directly to the receiver. The first arriving waves and the later arriving waves thus impose complementary information on the perturbation of the source position by constraining $(\hat{\mathbf{t}}\cdot\delta)$ and δ, respectively.

4. A Point Force in an Elastic Medium

[20] Let us now consider the displacement of a point force in an elastic medium. The far-field displacement due to a point force $\mathbf{F}$ at the origin in a homogeneous medium given by *Aki and Richards* [2002]:

$$\mathbf{u} = \frac{e^{ik_\alpha r}}{4\pi\rho\alpha^2 r}\hat{\mathbf{r}}(\hat{\mathbf{r}}\cdot\mathbf{F}) + \frac{e^{ik_\beta r}}{4\pi\rho\beta^2 r}(\mathbf{F}-\hat{\mathbf{r}}(\hat{\mathbf{r}}\cdot\mathbf{F}))\,, \tag{18}$$

where α and β are the P and S velocities, respectively, while the wave numbers are given by $k_\alpha = \omega/\alpha$ and $k_\beta = \omega/\beta$. For an arbitrary source spectrum $S(\omega)$, expression (18) should be multiplied with $S(\omega)$. For a source of finite spatial extent the source spectra of P and S waves may be different. In that case, the radiation patterns should also be corrected for a finite source size. Here we limit ourselves to sources with a spatial extent much smaller than a wavelength, such a source can be treated as a point source. This entails a limitation to weak events. In that case, $S(\omega)$ is the Fourier transform of the excitation, and this term is the same for P and S waves, so using the same reasoning that led to (13), we conclude that the source spectrum cancels. For this reason we suppress the presence of the source spectrum $S(\omega)$ altogether.

[21] When the source is displaced over a distance δ, the perturbation of the arrival time for the P waves is given by $-\alpha^{-1}(\hat{\mathbf{r}}\cdot\delta)$, while the perturbation of the arrival of the S waves is given by $-\beta^{-1}(\hat{\mathbf{r}}\cdot\delta)$. In the averages (5) and (7), the averages are taken with the intensities of each path as weight function. Since the P waves and the S waves can be considered to be different paths, the mean travel time perturbation is given by

$$\langle\tau\rangle = \frac{-\int\left|\frac{e^{ik_\alpha r}}{4\pi\rho\alpha^2 r}\hat{\mathbf{r}}(\hat{\mathbf{r}}\cdot\mathbf{F})\right|^2\frac{1}{\alpha}(\hat{\mathbf{r}}\cdot\delta)d\Omega - \int\left|\frac{e^{ik_\beta r}}{4\pi\rho\beta^2 r}(\mathbf{F}-\hat{\mathbf{r}}(\hat{\mathbf{r}}\cdot\mathbf{F}))\right|^2\frac{1}{\beta}(\hat{\mathbf{r}}\cdot\delta)d\Omega}{\int\left|\frac{e^{ik_\alpha r}}{4\pi\rho\alpha^2 r}\hat{\mathbf{r}}(\hat{\mathbf{r}}\cdot\mathbf{F})\right|^2 d\Omega + \int\left|\frac{e^{ik_\beta r}}{4\pi\rho\beta^2 r}(\mathbf{F}-\hat{\mathbf{r}}(\hat{\mathbf{r}}\cdot\mathbf{F}))\right|^2 d\Omega}\,. \tag{19}$$

Expression (19) can be simplified with the following identities: $|\hat{\mathbf{r}}(\hat{\mathbf{r}}\cdot\mathbf{F})|^2 = (\hat{\mathbf{r}}\cdot\hat{\mathbf{r}})^2(\hat{\mathbf{r}}\cdot\mathbf{F})^2 = (\hat{\mathbf{r}}\cdot\mathbf{F})^2$ and $|(\mathbf{F}-\hat{\mathbf{r}}(\hat{\mathbf{r}}\cdot\mathbf{F}))|^2 = F^2 - 2(\hat{\mathbf{r}}\cdot\mathbf{F})(\hat{\mathbf{r}}\cdot\mathbf{F}) + (\hat{\mathbf{r}}\cdot\hat{\mathbf{r}})(\hat{\mathbf{r}}\cdot\mathbf{F})^2 = F^2 - (\hat{\mathbf{r}}\cdot\mathbf{F})^2$. Using these identities gives

$$\langle\tau\rangle = \frac{-\int\frac{1}{\alpha^4}(\hat{\mathbf{r}}\cdot\mathbf{F})^2\frac{1}{\alpha}(\hat{\mathbf{r}}\cdot\delta)d\Omega - \int\frac{1}{\beta^4}\left(F^2-(\hat{\mathbf{r}}\cdot\mathbf{F})^2\right)^2\frac{1}{\beta}(\hat{\mathbf{r}}\cdot\delta)d\Omega}{\int\frac{1}{\alpha^4}(\hat{\mathbf{r}}\cdot\mathbf{F})^2 d\Omega + \int\frac{1}{\beta^4}\left(F^2-(\hat{\mathbf{r}}\cdot\mathbf{F})^2\right)d\Omega}\,. \tag{20}$$

Both integrals in the numerator vanish because the integrands are odd functions of $\hat{\mathbf{r}}$ and the integration is carried out over the full unit sphere; therefore $\langle\tau\rangle = 0$.

[22] The variance in the travel time can be computed by replacing $-\alpha^{-1}(\hat{\mathbf{r}}\cdot\delta)$ in the numerator by $\alpha^{-2}(\hat{\mathbf{r}}\cdot\delta)^2$ and $-\beta^{-1}(\hat{\mathbf{r}}\cdot\delta)$ by $\beta^{-2}(\hat{\mathbf{r}}\cdot\delta)^2$. This gives

$$\sigma_\tau^2 = \frac{\int\frac{1}{\alpha^6}(\hat{\mathbf{r}}\cdot\mathbf{F})^2(\hat{\mathbf{r}}\cdot\delta)^2 d\Omega + \int\frac{1}{\beta^6}\left(F^2-(\hat{\mathbf{r}}\cdot\mathbf{F})^2\right)^2(\hat{\mathbf{r}}\cdot\delta)^2 d\Omega}{\int\frac{1}{\alpha^4}(\hat{\mathbf{r}}\cdot\mathbf{F})^2 d\Omega + \int\frac{1}{\beta^4}\left(F^2-(\hat{\mathbf{r}}\cdot\mathbf{F})^2\right)d\Omega}\,, \tag{21}$$

or, equivalently,

$$\sigma_\tau^2 = \frac{\left(\frac{1}{\alpha^6}-\frac{1}{\beta^6}\right)\int(\hat{\mathbf{r}}\cdot\mathbf{F})^2(\hat{\mathbf{r}}\cdot\delta)^2 d\Omega + \frac{F^2}{\beta^6}\int(\hat{\mathbf{r}}\cdot\delta)^2 d\Omega}{\left(\frac{1}{\alpha^4}-\frac{1}{\beta^4}\right)\int(\hat{\mathbf{r}}\cdot\mathbf{F})^2 d\Omega + \frac{F^2}{\beta^4}\int d\Omega}\,. \tag{22}$$

The integrations over the unit sphere can be carried out using representation (16) for $\hat{\mathbf{r}}$. It is convenient to align the z axis with the point force $\mathbf{F}$, so that $(\hat{\mathbf{r}}\cdot\mathbf{F}) = F\cos\theta$. For that coordinate system, the first integral in the numerator is given by

$$\begin{aligned}\int(\hat{\mathbf{r}}\cdot\mathbf{F})^2(\hat{\mathbf{r}}\cdot\delta)^2 d\Omega &= F^2\delta_x^2\int_0^{2\pi}\int_0^{\pi}\sin^2\theta\cos^2\varphi\cos^2\theta\sin\theta d\theta d\varphi\\ &+ F^2\delta_y^2\int_0^{2\pi}\int_0^{\pi}\sin^2\theta\sin^2\varphi\cos^2\theta\sin\theta d\theta d\varphi\\ &+ F^2\delta_z^2\int_0^{2\pi}\int_0^{\pi}\cos^2\theta\cos^2\theta\sin\theta d\theta d\varphi\\ &= \frac{4\pi}{15}F^2\left(\delta_x^2+\delta_y^2\right)+\frac{4\pi}{5}F^2\delta_z^2\,.\end{aligned} \tag{23}$$

Equation (23) holds for the special case of a coordinate system that is aligned with the point force. The last line can be rewritten as

$$\frac{4\pi}{15}F^2\left(\delta_x^2+\delta_y^2\right)+\frac{4\pi}{5}F^2\delta_z^2=\frac{4\pi}{15}F^2\left(\delta_x^2+\delta_y^2+\delta_z^2\right)+4\pi\left(\frac{1}{5}-\frac{1}{15}\right)F^2\delta_z^2=\frac{4\pi}{15}F^2\delta^2+\frac{8\pi^2}{15}\left(\mathbf{F}\cdot\delta\right)^2. \quad (24)$$

The last identity is invariant under unitary coordinate transformations such as rotations; therefore expression (24) holds in any coordinate system.

[23] Applying a similar analysis to all terms in (22) gives, after dividing by F^2 and some rearrangement,

$$\sigma_\tau^2=\frac{\left(\frac{1}{\alpha^6}+\frac{4}{\beta^6}\right)\delta^2-2\left(\frac{1}{\beta^6}-\frac{1}{\alpha^6}\right)\left(\hat{\mathbf{F}}\cdot\delta\right)^2}{5\left(\frac{1}{\alpha^4}+\frac{2}{\beta^4}\right)}, \quad (25)$$

where $\hat{\mathbf{F}}\equiv\mathbf{F}/F$ is the unit vector in the direction of the point force.

[24] Note that for the elastic wave generated by a point force, $\langle\sigma_\tau^2\rangle$ depends on not just δ^2 but also on $\left(\hat{\mathbf{F}}\cdot\delta\right)$, the projection of the source displacement along the point force. Therefore the direction of the point force is needed in order to relate the observed value of $\langle\sigma_\tau^2\rangle$ to the source displacement. This contrasts with the acoustic case treated in section 3 where the variance of the travel time was dependent on δ only.

[25] For a Poisson medium ($\alpha=\sqrt{3}\beta$), expression (24) results in

$$\sigma_\tau^2\approx\frac{\delta^2}{\beta^2}\left(0.382-0.182\left(\hat{\mathbf{F}}\cdot\hat{\delta}\right)^2\right) \quad (26)$$

(Poisson medium). Note that the last term is rewritten in terms of the unit vector $\hat{\delta}$. The first term gives the contribution that is direction-independent. For the acoustic case the corresponding result (17) is $\langle\sigma_\tau^2\rangle=\delta^2/3v^3\approx 0.333\delta^2/v^2$, which is close to the coefficient 0.382 in (26) when the shear velocity β is equated to the velocity v in the acoustic medium. There is a simple reason for this. In expression (25) the velocities α and β are raised to a fairly high negative power (-4 and -6, respectively). Since $\beta<\alpha$, this leads to a dominance of the terms that are dependent on β. In fact, when the α-dependent terms in (25) are ignored altogether, expression (25) reduces to

$$\sigma_\tau^2\approx\frac{\delta^2}{\beta^2}\left(0.4-0.2\left(\hat{\mathbf{F}}\cdot\hat{\delta}\right)^2\right) \quad (27)$$

(α ignored). This crude approximation leads to a result that is close to (26) for a Poisson medium. Physically, this happens because a point force excites much stronger S waves than P waves. Since the travel time averages are weighted with the intensity of both wave types, the contribution of the shear waves dominates. The dominance of the S wave energy over the P wave energy has been noted before in different contexts [*Aki and Chouet*, 1975; *Weaver*, 1982; *Papanicolaou and Ryzhik*, 1999; *Trégourès and van Tiggelen*, 2002; *Snieder*, 2002].

[26] The analysis used in this paper is slightly oversimplified because it does not account for the different scattering cross sections for incoming P waves and incoming S waves. According to *Wu and Aki* [1985] these cross sections have the following dependence on the P and S velocities: $g_{P\to P}\sim 1/\alpha^4$, $g_{P\to S}\sim 1/\beta^4$, $g_{S\to P}\sim 1/\alpha^4$, and $g_{S\to S}\sim 1/\beta^4$. For an incoming P wave, the total scattering cross section is proportional to $g_{P\to P}+g_{P\to S}$. Since these terms depend on the fourth power of the velocities and because $\beta<\alpha$, $g_{P\to P}+g_{P\to S}\sim 1/\beta^4$, up to a relative error of the order $(\beta/\alpha)^4\sim 0.1$. For the same reason, the total scattering cross section for an incoming S wave is given by $g_{S\to P}+g_{S\to S}$, which also is approximately proportional to $1/\beta^4$. This means that for both incoming P waves and incoming S waves the outgoing S wave dominates and for each trajectory gives a common factor $1/\beta^4$ that cancels in the numerator and denominator of expression (20) and subsequent expression for the mean travel time perturbation and its variance.

[27] In some situations one can eliminate the dependence of the variance of the travel time on the direction of the source displacement. As an example, consider a vibrator in a borehole that vibrates in a direction perpendicular to the borehole. The relative location of different deployments of the vibrator depends only on the distance along the borehole. In that case the force $\mathbf{F}$ and the source displacement δ are perpendicular, and equation (25) reduces to

$$\sigma_\tau^2=\frac{\left(\frac{1}{\alpha^6}+\frac{4}{\beta^6}\right)}{5\left(\frac{1}{\alpha^4}+\frac{2}{\beta^4}\right)}\delta^2 \qquad (\mathbf{F}\perp\delta). \quad (28)$$

Of course, one may question the validity of the employed model for a source in a borehole since the presence of the borehole and the properties of its walls modify the radiation of elastic waves.

5. A Moment Tensor Source in an Elastic Medium

[28] In this section we consider the displacement caused by a moment tensor source in an elastic medium. In section 5.1 we consider the case of a double couple, and in section 5.2 we consider that of an explosive source. According to *Aki and Richards* [2002], the displacement in an elastic medium due to a moment tensor source $\mathbf{M}$ is given by

$$u_i(\mathbf{r})=-\frac{i\omega e^{ik_\alpha r}}{4\pi\rho\alpha^3 r}\hat{r}_i\hat{r}_j\hat{r}_k M_{jk}-\frac{i\omega e^{ik_\beta r}}{4\pi\rho\beta^3 r}\left(\hat{r}_i\hat{r}_j\hat{r}_k M_{jk}-\delta_{ij}\hat{r}_k M_{jk}\right). \quad (29)$$

Following expression (5), the travel time perturbation for each trajectory is weighted by the intensity for that trajectory. The intensity corresponding to the different terms in (29) can be computed using the identities $\left(\hat{r}_i\hat{r}_j\hat{r}_k M_{jk}\right)^2=(\hat{\mathbf{r}}\cdot\hat{\mathbf{r}})^2(\hat{\mathbf{r}}\hat{\mathbf{r}}:\mathbf{M})^2=(\hat{\mathbf{r}}\hat{\mathbf{r}}:\mathbf{M})^2$, and $\left(\hat{r}_i\hat{r}_j\hat{r}_k M_{jk}-\delta_{ij}\hat{r}_k M_{jk}\right)^2=(\hat{\mathbf{r}}\cdot\mathbf{M})^2-(\hat{\mathbf{r}}\hat{\mathbf{r}}:\mathbf{M})^2$. By analogy with expression (20) the

mean travel time change due to a perturbation δ in the source location is given by

$$\langle\tau\rangle = \frac{-\int\frac{1}{\alpha^6}(\hat{\mathbf{r}}\hat{\mathbf{r}}:\mathbf{M})^2\frac{1}{\alpha}(\hat{\mathbf{r}}\cdot\delta)d\Omega - \int\frac{1}{\beta^6}\Big((\hat{\mathbf{r}}\cdot\mathbf{M})^2-(\hat{\mathbf{r}}\hat{\mathbf{r}}:\mathbf{M})^2\Big)\frac{1}{\beta}(\hat{\mathbf{r}}\cdot\delta)d\Omega}{\int\frac{1}{\alpha^6}(\hat{\mathbf{r}}\hat{\mathbf{r}}:\mathbf{M})^2 d\Omega + \int\frac{1}{\beta^6}\Big((\hat{\mathbf{r}}\cdot\mathbf{M})^2-(\hat{\mathbf{r}}\hat{\mathbf{r}}:\mathbf{M})^2\Big)d\Omega} . \tag{30}$$

Just as is the integral (20), the integrand is an odd function of $\hat{\mathbf{r}}$, and the integral vanishes upon integration over the unit sphere so the mean travel time perturbation vanishes: $\langle\tau\rangle = 0$. Using the same reasoning as that used for (21), the variance of the travel time is given by

$$\sigma_\tau^2 = \frac{\int\frac{1}{\alpha^8}(\hat{\mathbf{r}}\hat{\mathbf{r}}:\mathbf{M})^2(\hat{\mathbf{r}}\cdot\delta)^2 d\Omega + \int\frac{1}{\beta^8}\Big((\hat{\mathbf{r}}\cdot\mathbf{M})^2-(\hat{\mathbf{r}}\hat{\mathbf{r}}:\mathbf{M})^2\Big)(\hat{\mathbf{r}}\cdot\delta)^2 d\Omega}{\int\frac{1}{\alpha^6}(\hat{\mathbf{r}}\hat{\mathbf{r}}:\mathbf{M})^2 d\Omega + \int\frac{1}{\beta^6}\Big((\hat{\mathbf{r}}\cdot\mathbf{M})^2-(\hat{\mathbf{r}}\hat{\mathbf{r}}:\mathbf{M})^2\Big)d\Omega} . \tag{31}$$

The integration over the unit sphere is most easily carried out when a simplified form of the moment tensor is assumed.

5.1. A Double-Couple Source

[29] In this section we analyze the variance of the travel time for a double-couple source. In the integration we use a coordinate system with the z axis perpendicular to the double couple. In that coordinate system the moment tensor is given by

$$\mathbf{M} = \begin{pmatrix} 0 & M & 0 \\ M & 0 & 0 \\ 0 & 0 & 0 \end{pmatrix} . \tag{32}$$

With representation (16) for the unit vector $\hat{\mathbf{r}}$, the contractions that appear in (31) are given by

$$(\hat{\mathbf{r}}\cdot\mathbf{M})^2 = M^2\sin^2\theta , \tag{33}$$

$$(\hat{\mathbf{r}}\hat{\mathbf{r}}:\mathbf{M})^2 = 4M^2\sin^4\theta\sin^2\varphi\cos^2\varphi . \tag{34}$$

With these representations the angular integrals that appear in (31) can be carried out. The resulting integrals are tedious and are given by

$$\int(\hat{\mathbf{r}}\cdot\mathbf{M})^2 d\Omega = \frac{8\pi}{3}M^2 , \tag{35}$$

$$\int(\hat{\mathbf{r}}\hat{\mathbf{r}}:\mathbf{M})^2 d\Omega = \frac{16\pi}{15}M^2 , \tag{36}$$

$$\int(\hat{\mathbf{r}}\cdot\mathbf{M})^2(\hat{\mathbf{r}}\cdot\delta)^2 d\Omega = \frac{16\pi}{15}M^2\Big(\delta_x^2+\delta_y^2\Big) + \frac{8\pi}{15}M^2\delta_z^2 , \tag{37}$$

$$\int(\hat{\mathbf{r}}\hat{\mathbf{r}}:\mathbf{M})^2(\hat{\mathbf{r}}\cdot\delta)^2 d\Omega = \frac{16\pi}{35}M^2\Big(\delta_x^2+\delta_y^2\Big) + \frac{16\pi}{105}M^2\delta_z^2 . \tag{38}$$

Inserting these results in expression (33) and using the identity $\delta_x^2 + \delta_y^2 = \delta^2 - \delta_z^2$ gives after a rearrangement of terms

$$\sigma_\tau^2 = \frac{\Big(\frac{6}{\alpha^8}+\frac{7}{\beta^8}\Big)\delta^2 - \Big(\frac{4}{\alpha^8}+\frac{3}{\beta^8}\Big)\delta_z^2}{7\Big(\frac{2}{\alpha^6}+\frac{3}{\beta^6}\Big)} . \tag{39}$$

Expression (39) is not quite satisfactory yet because it does not contain the moment tensor in a covariant form. (The only information of the orientation of the double couple is captured in the choice of the z direction, which is orthogonal to the double couple.) A covariant formulation can be obtained by defining the following norm of the moment tensor:

$$\|\mathbf{M}\|^2 \equiv (\mathbf{M}:\mathbf{M}) . \tag{40}$$

Since this quantity is the double contraction of a tensor of rank two, it is a tensor of rank zero; hence $\|\mathbf{M}\|$ is invariant for unitary coordinate transforms. With this norm we can define a normalized moment tensor

$$\hat{\mathbf{M}} \equiv \frac{\mathbf{M}}{\|\mathbf{M}\|} . \tag{41}$$

Since $\mathbf{M}$ is a tensor of rank two and $\|\mathbf{M}\|$ is a scalar, $\hat{\mathbf{M}}$ is a tensor of rank two. For the moment tensor (32),

$$\big(\hat{\mathbf{M}}\cdot\delta\big)^2 = \frac{1}{2}\big(\delta^2-\delta_z^2\big) . \tag{42}$$

This result can be used to eliminate δ_z from expression (39) so that

$$\sigma_\tau^2 = \frac{\Big(\frac{2}{\alpha^8}+\frac{4}{\beta^8}\Big)\delta^2 + 2\Big(\frac{4}{\alpha^8}+\frac{3}{\beta^8}\Big)\big(\hat{\mathbf{M}}\cdot\delta\big)^2}{7\Big(\frac{2}{\alpha^6}+\frac{3}{\beta^6}\Big)} . \tag{43}$$

Expression (43) is invariant for rotations of the coordinate system and can therefore be applied to a double couple with an arbitrary orientation.

[30] Just as with expression (25) for a point force, the variance of the travel time depends on the magnitude δ of the source displacement as well as on the direction of the source displacement. Therefore it is necessary to know the orientation of the double couple in order to relate the variance in the travel time perturbation as inferred from coda wave interferometry to the source displacement.

[31] For a Poisson medium

$$\sigma_\tau^2 \approx \frac{\delta^2}{\beta^2}\Big(0.187 + 0.283\Big(\hat{\mathbf{M}}\cdot\hat{\delta}\Big)^2\Big) . \tag{44}$$

(Poisson medium). A comparison with expression (26) for a point force shows that the ratio of the isotropic term to the direction-dependent term is, relatively speaking, smaller for the double couple than for the point force. The reason is that

for the double couple the angular variation in the radiation pattern is larger than that for a point force.

[32] Equation (43) contains terms that depend on the P velocity and those that depend on the S velocity. When the contributions of the P waves are ignored altogether, the variance of the travel time change is given by

$$\sigma_\tau^2 \approx \frac{\delta^2}{\beta^2}\left(0.190 + 0.285\left(\hat{\mathbf{M}}\cdot\hat{\delta}\right)^2\right) \tag{45}$$

(α ignored). Note that this result is close to the variance of the travel time for a Poisson medium given in (44). For a double couple the radiated energy varies as β^{-6}, whereas for a point force it varies as β^{-4}. For this reason the dominance of the S waves in coda wave interferometry is even more pronounced for a double couple than for a point force.

[33] As a special case, let us consider the application of this theory to the relative location of aftershocks on a fault. In that case, the relative source location δ lies in the fault plane. In the coordinate system used in expression (39), the x, y plane is aligned with the fault plane and the component δ_z perpendicular to the fault plane is equal to zero so that

$$\sigma_\tau^2 = \frac{\left(\frac{6}{\alpha^8}+\frac{7}{\beta^8}\right)}{7\left(\frac{2}{\alpha^6}+\frac{3}{\beta^6}\right)}\delta^2 \tag{46}$$

(displacement in fault plane). Just as in expression (28) the variance of the travel time perturbation is now related to the absolute value of the source displacement only. Note that when the P wave terms in expression (46) are ignored, that expression is given by $\sigma_\tau^2 = \delta^2/3\beta^2$. Expression (46) is equal to equation (17) for an explosive source in an acoustic medium. This resemblance is, however, fortuitous.

5.2. An Explosive Source

[34] For an explosive source, the moment tensor is given by

$$\mathbf{M} = \begin{pmatrix} M & 0 & 0 \\ 0 & M & 0 \\ 0 & 0 & M \end{pmatrix}. \tag{47}$$

For such a moment tensor $(\hat{\mathbf{r}}\hat{\mathbf{r}} : \mathbf{M})^2 = M^2\hat{r}_i\hat{r}_j\delta_{ij} = M^2(\hat{\mathbf{r}}\cdot\hat{\mathbf{r}})^2 = M^2$, and $(\hat{\mathbf{r}}\cdot\mathbf{M})^2 = (\hat{\mathbf{r}}\cdot\hat{\mathbf{r}})^2M^2 = M^2$, so that (31) is given by

$$\sigma_\tau^2 = \frac{\int \frac{1}{\alpha^8}(\hat{\mathbf{r}}\cdot\delta)^2 d\Omega}{\int \frac{1}{\alpha^6} d\Omega}. \tag{48}$$

Note that the terms that depend on the shear velocity β have disappeared; physically, this is because an explosive source does not excite shear waves. The angular integration can be carried out in the same way as in section 3, so that

$$\sigma_\tau^2 = \frac{1}{3}\frac{\delta^2}{\alpha^2}. \tag{49}$$

This result is identical to expression (17) for acoustic waves.

6. Application to Relative Source Location

[35] As shown in the previous sections, the cross correlation of the coda waves carries information of the source displacement. The cross correlation (3) can be applied to a number of nonoverlapping time windows in the seismic coda. Using expression (6), each of these windows gives an independent estimate of the variance σ_τ^2.

[36] Let us first consider the character of the constraints on the source displacement that follow from coda wave interferometry. For an explosive source in either an acoustic or elastic medium, expressions (17) and (49) state that the source displacement is located on a sphere with radius $\delta^2/3v^2$, with v the velocity of acoustic waves for an acoustic medium and the P wave velocity for an elastic medium, respectively.

[37] For a point force in an elastic medium the constraint on the source location is slightly more complicated. It is possible to decompose the source displacement into a component parallel to the point force and a component perpendicular to the point force:

$$\delta = \delta_{\perp F} + \delta_{\parallel F}\hat{\mathbf{F}}. \tag{50}$$

With this decomposition, equation (25) can be written as

$$\sigma_\tau^2 = \frac{\left(\frac{1}{\alpha^6}+\frac{4}{\beta^6}\right)\delta_{\perp F}^2 + \left(\frac{3}{\alpha^6}+\frac{2}{\beta^6}\right)\delta_{\parallel F}^2}{5\left(\frac{1}{\alpha^4}+\frac{2}{\beta^4}\right)}. \tag{51}$$

Expression (51) states the source displacement is located on an ellipsoid whose symmetry axis is aligned with the point force.

[38] For a double couple the source displacement can be decomposed in a component $\delta_{\parallel\text{fault}}$ parallel to the fault and a component $\delta_{\perp\text{fault}}$ perpendicular to the fault. Following equation (39), the corresponding constraint on the source displacement is given by

$$\sigma_\tau^2 = \frac{\left(\frac{6}{\alpha^8}+\frac{7}{\beta^8}\right)\delta_{\parallel\text{fault}}^2 + 2\left(\frac{1}{\alpha^8}+\frac{2}{\beta^8}\right)\delta_{\perp\text{fault}}^2}{7\left(\frac{2}{\alpha^6}+\frac{3}{\beta^6}\right)}. \tag{52}$$

Expression (52) states that the source displacement is located on an ellipsoid with a symmetry axis perpendicular to the fault plane. In the special case of aftershocks that occur on the same fault, the source displacement is in general in the plane of the fault. In that case the source displacement is constrained to be located on a circle in the fault plane:

$$\sigma_\tau^2 = \frac{\left(\frac{6}{\alpha^8}+\frac{7}{\beta^8}\right)}{7\left(\frac{2}{\alpha^6}+\frac{3}{\beta^6}\right)}\delta_{\parallel\text{fault}}^2. \tag{53}$$

[39] In all these situations the source displacement is constrained by coda wave interferometry to be located on a sphere, an ellipsoid, or a circle. This constraint can be used in addition to constraints on the relative source location as inferred from the differential arrival times for the P and S waves. Coda wave interferometry thus adds a

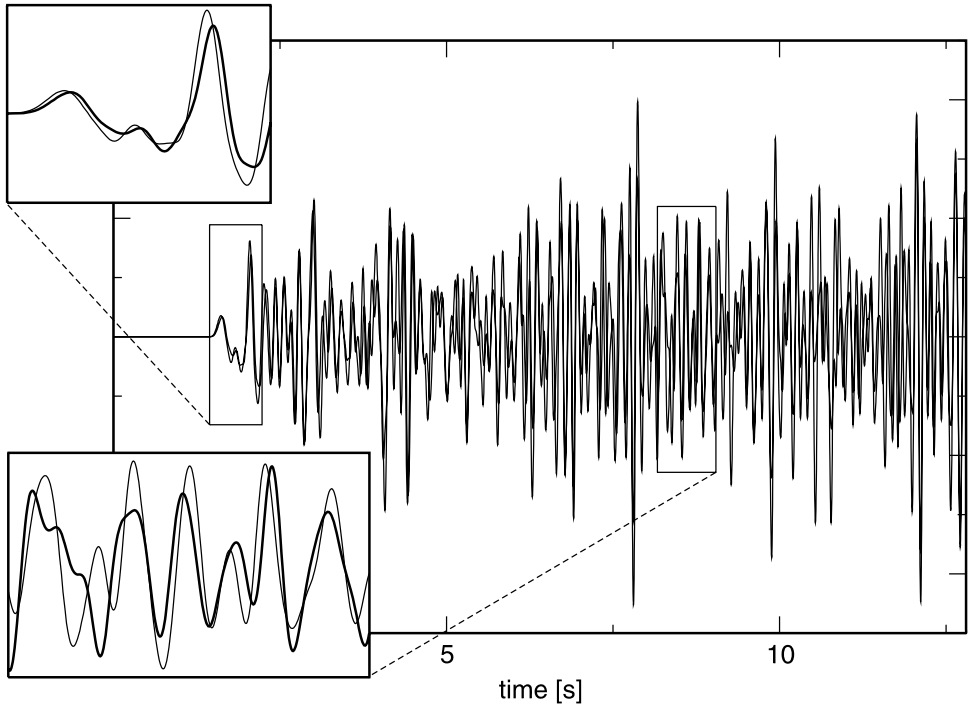

Figure 2. Synthetic seismograms for two source locations recorded at the same receiver. The top and bottom inserts show close-ups of the direct arrivals and a section of the coda, respectively.

geometrical constraint to the relative source locations of multiple events.

7. Validation With Synthetic Seismograms

[40] In order to validate the theory we present an experiment where synthetic seismograms are computed with an acoustic finite difference algorithm. The two-dimensional computational grid is 20 km by 20 km with a grid size of 20 m. The source emits a Ricker wavelet with a dominant frequency of 8 Hz. The density is constant, while the velocity model consists of the superposition of a constant background velocity of 6000 m/s with a realization of a Gaussian random medium with a correlation length of 1000 m and a standard deviation of 1500 m/s. These fluctuations constitute a perturbation of 25% and lead to strong multiple scattering.

[41] Synthetic seismograms for one receiver at two source positions that are 160 m apart are shown in Figure 2. The amplitude of the direct wave is small compared to the coda, and the coda is enriched in high frequencies compared to the direct wave; this is due to the strong scattering. Figure 2 insets show the direct arrival and part of the coda. The first part of the waveforms is similar with a small lag between the waveforms; this time lag forms the basis of the double-difference method.

[42] Here we use the coda to extract the separation in the source position by computing the cross correlation (3) using a time window with a length of 1.6 s. We compute the cross correlation as a function of time by sliding the time window along the waveforms. The variance in the travel time due to the source displacement follows from expression (6). The source displacement follows from the generalization of equation (17) to two spatial dimensions where it is given by

$$\sigma_\tau^2 = \frac{1}{2}\frac{\delta^2}{v^2} \; . \tag{54}$$

[43] The maximum of the normalized cross correlation of the seismograms recorded at one station for two nearby source locations is shown in Figure 3 as a function of the center time of the time window. Figure 3 (top) shows the two seismograms. The horizontal bar indicates the size of the time window used to compute the cross correlation. The maximum of the cross correlation ($R_{\max}$) for each time window is shown in Figure 3 (middle). The high values of $R_{\max}$ at early times correspond to the high degree of similarity in the first arrivals that indicates that the source mechanism for the two events is similar. For later times, around $t = 4$ s, $R_{\max}$ decreases as the time window moves into the coda. The computed distance is shown in Figure 3 (bottom). The dashed line indicates the actual source displacement of 160 m.

[44] For center times later than about 4 s the source separation inferred from the coda fluctuates around the actual source separation of 160 m. For earlier times the correlation of the waveforms leads to an underestimation of the source separation. The reason for this is that for early times the scattered waves did not have the time to propagate in all directions as indicated in Figure 1, this means that for these times the employed model where the scattered waves are integrated over all takeoff angles is not accurate.

[45] The source separation can be computed for nonoverlapping time windows. This gives independent estimates of the source separation that provide a consistency check for

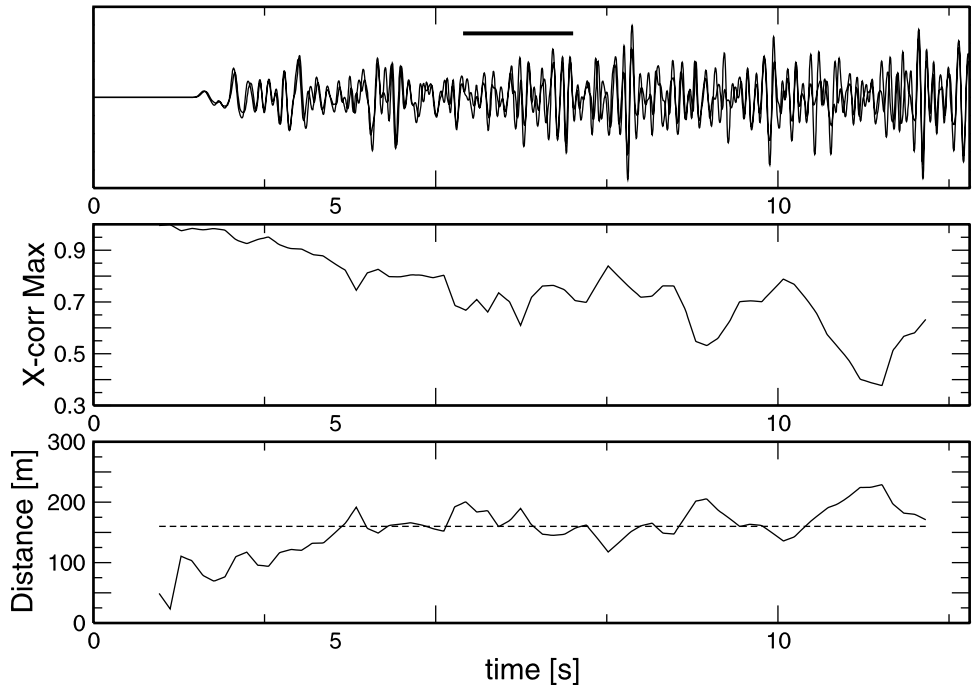

Figure 3. (middle) Maximum of the cross correlation and (bottom) calculated distance for the seismograms in Figure 2 as a function of the center time of the time window used for computing the cross correlation. (top) Two seismograms. The horizontal bar indicates the size of the time window in which we compute the cross correlation. The dashed line in the bottom insert gives the true source separation.

the employed method. These independent estimates can be used to obtain an error estimate of the inferred source separation. The method to compute the source separation from the coda waves is based on the cross correlation of the waveforms only. It is not necessary to know the scattering properties of the medium.

[46] The synthetics used in Figure 3 are noise-free. Nevertheless, the estimated source separation shown in Figure 3 (bottom) fluctuates as a function of the center time of the employed time window. As mentioned in section 2, coda wave interferometry ignores the contribution to the cross correlation that is due to waves that propagate along different trajectories. The associated cross terms lead to the fluctuations shown in Figure 3 (bottom). *Snieder* [2004a] show that the relative contribution of these cross terms is of the order $\sqrt{t_{corr}/t_w}$, where $2t_w$ is the employed window length and $t_{\rm corr}$ is the width of the autocorrelation of the data. Choosing a larger window length reduces these fluctuations at the expense of having fewer independent estimates of the source separation.

8. Application to Earthquake Doublets on the Hayward Fault

[47] We apply the theory to measure the source separation for earthquakes on the Hayward fault, California, using coda waves recorded by the Northern California Seismic Network [*Waldhauser and Ellsworth*, 2000]. They constructed an algorithm (double-difference algorithm) that inverts for hypocenter locations using absolute and relative travel time measurements. The double-difference algorithm minimizes residuals between observed and theoretical travel times (double differences) for a large data set. We compare our results to the results of this inversion.

[48] We filtered the waveforms with a band-pass Butterworth filter, filtering out the DC component and frequencies greater than 5 Hz. This decreases the dominant frequency to an average of 3 Hz. We align the seismograms in time so that the first arrivals coincide. This affects the lag of the cross correlation but not its maximum $R_{\rm max}$. Figure 4 shows two events that occurred close together and were recorded at the same station.

[49] In Figure 4 one of the two seismograms is scaled because of a difference in magnitude between the two events. As for the synthetics of Figure 2, the first arrivals are similar. This implies that the source mechanism for both events is similar. There is a magnitude difference because the earthquakes are of different magnitude, but this does not affect the value of the normalized cross correlation.

[50] We choose the time window for the cross correlation (3) to be 10 s. A pair of seismograms for the events 238295 and 242003 recorded at the same station is shown in Figure 5 (top). Figure 5 (middle) shows the maximum $R_{\rm max}$ of the cross correlation as a function of the center time of the time window. In Figure 4 the noise is appreciable because the waves arriving before the first direct P wave are significant. Random noise added to the waveforms reduces the cross correlation and therefore leads to an overestimation of the source separation. Appendix B summarizes the treatment of H. Douma and R. Snieder (The imprint of noise on the cross correlation of time series, with applications to coda wave interferometry, submitted to *Geophysical Journal International*, 2004, hereinafter referred to as Douma and Snieder, submitted manuscript, 2004), in which

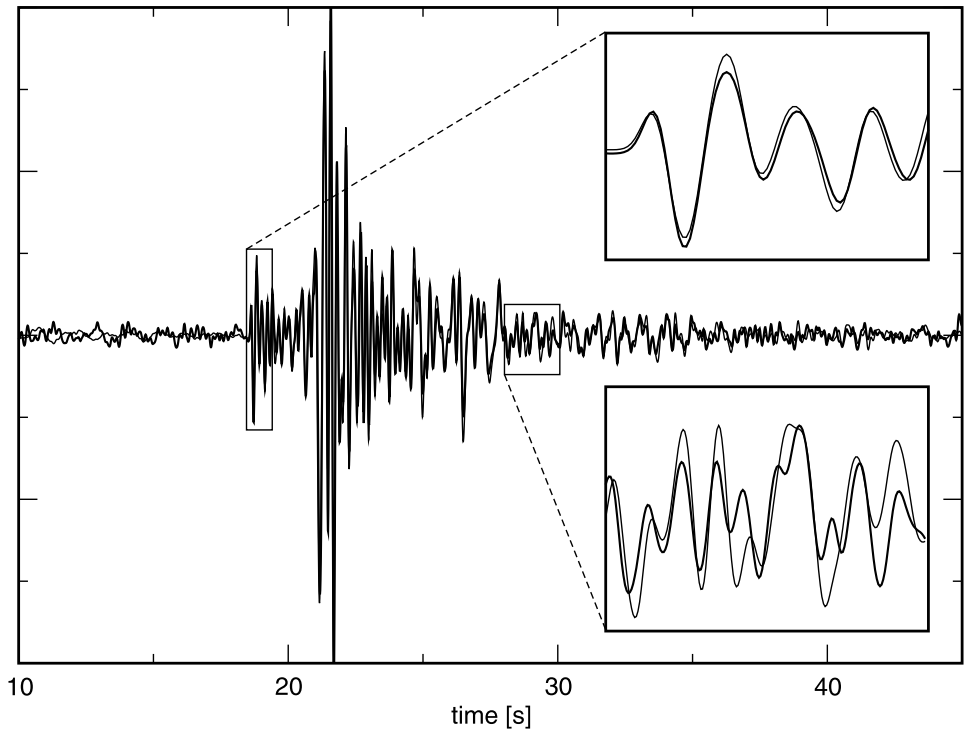

Figure 4. Seismograms from an earthquake doublet recorded at the same station. The top and bottom inserts show close-ups of the direct arrivals and a section of the coda, respectively. One of the two seismograms is scaled because of a difference in magnitude between the events.

it is shown that the bias in the cross correlation due to random noise can be corrected for by using the corrected cross correlation coefficient that is given by

$$R_{\text{corr}} = R \Big/ \sqrt{1 - \frac{\langle n_1^2 \rangle}{\langle u_1^2 \rangle}} \sqrt{1 - \frac{\langle n_2^2 \rangle}{\langle u_2^2 \rangle}}. \tag{55}$$

In expression (55), R is the normalized correlation coefficient defined in expression (3), $\langle n_{1,2}^2 \rangle$ gives the average noise energy in the unperturbed and perturbed waves, while $\langle u_{1,2}^2 \rangle$ gives the average energy of the unperturbed and perturbed waves employed in the time window. We show in Figure B1 of Appendix B that with noise-contaminated data it is crucial to correct the correlation coefficient for the bias introduced by random noise.

[51] We correct for random noise using expression (55). The variance of the travel time perturbation due to the source perturbation then follows from expression (6). Assuming that the events are taking place on the same fault plane we then use equation (46) to compute the source separation. In Figure 5 (bottom) we show the computed distance between the two events using the values β = 3320 m/s, and α = 5750 m/s that were also used by *Waldhauser and Ellsworth* [2002]. The dashed lines indicate the event separation obtained by *Waldhauser and Ellsworth* [2002] plus and minus one standard deviation. For center times smaller than about 40 s the distance calculated from coda waves agrees with the double-difference distance. For later times the distance computed from the coda waves overestimates the event separation. The reason for this is that for these late times the coda waves are so weak that the waveforms are dominated by random noise. When the noise is uncorrelated the cross correlation of the waveforms vanishes, and the variance of the travel time perturbation is according to expression (6) given by $\sigma_\tau^2 = 2/\overline{\omega^2}$. This variance depends on the frequency content only and is not related in any way to the event separation. For earlier times when the signal-to-noise ratio is not too low, the event separation computed from the coda waves agrees well with the event separation computed with the double-difference method.

[52] Note that the event separation shown in Figure 5 (bottom) is determined from data from a single station. By applying the method to event pairs recorded at several stations one obtains independent estimates of the event separation that can be used to estimate the uncertainty in the event separation. For events 238295 and 242003 that are shown in Figure 5, the event separation computed from waveforms recorded at the stations CAI, CBW, CMC, and CSP are shown in Figure 6 (top). We computed the mean event separation and its variance by averaging the event separation obtained from several nonoverlapping time windows at a single station, and by averaging over the event separation obtained from measurements at different stations. This leads to the average event separation and variance shown in Table 1. Table 1 gives the event separation and variance obtained with the double-difference method [*Waldhauser and Ellsworth*, 2002].

[53] In Figure 6 and in Table 1 this estimate of the event separation and its variance is shown for three different event pairs. The event separation obtained from coda wave interferometry and from the double-difference method agree

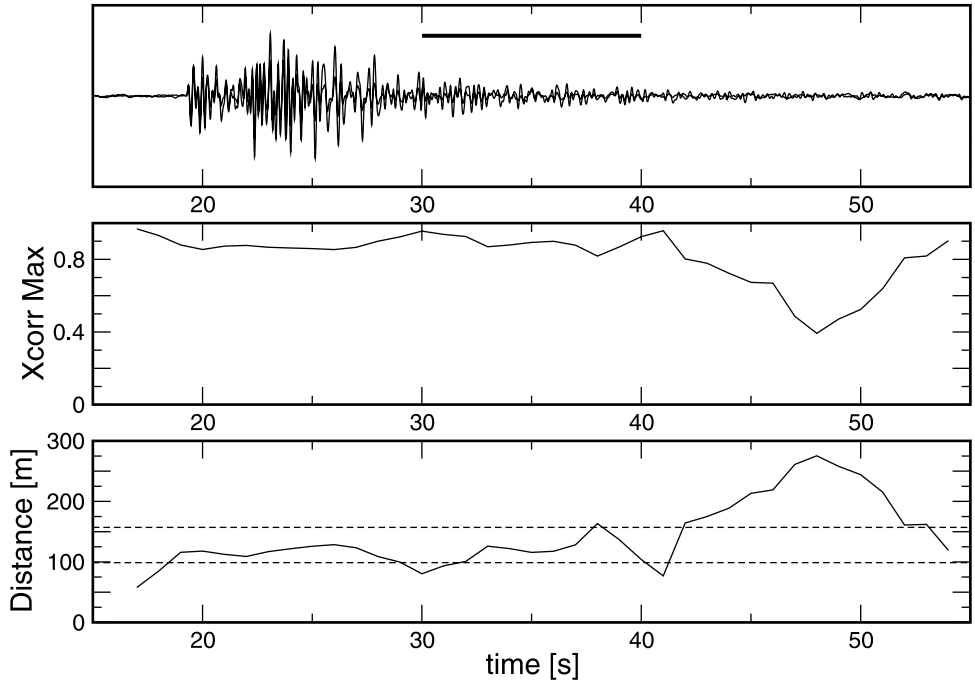

Figure 5. (top) Seismograms of events 23895 and 242003 recorded at the station CAI. (middle) Noise-corrected cross correlation as a function of the center time of the time window. (bottom) Estimated source separation as a function of the center time shown by the solid line. The dashed lines indicate the relative distance obtained by *Waldhauser and Ellsworth* [2002] plus or minus one standard deviation.

within one standard deviation. It is not clear at this point which of the methods provides the most accurate estimate of the event separation.

9. Discussion

[54] The method proposed in this paper makes it possible to compute the distance between seismic events with the same source mechanism using the seismic coda recorded for the two events at a single station. The theory is based on the assumption that the waves radiate from the source in all possible directions toward the scatterers that generate the coda. Note that the scattering properties of the medium do not need to be known; there is no need to prescribe the scattering mean free path or other parameters that characterize the scattering process.

[55] The theory presented here is based on the assumption that the scatterer density is constant in all directions from the source. In practice this assumption may be violated. Suppose, for example, that the source is displaced toward a region that is enriched in scatterers. The travel times along the trajectories to that region will decrease. The averages in the expressions (5) and (7) are weighted by the intensity. The trajectories to the region with strong scattering region dominate this average, which for this particular example leads to a negative mean travel time change. This would be visible as a nonzero phase shift of the coda waves. Neither the synthetic waveforms of Figure 2 nor the data of Figure 4 display such a phase shift.

[56] The derivation used here is based on a number of simplifications. We have assumed that the velocity is isotropic. If this is not the case expression (9) must be modified to include the dependence of the seismic velocity on the takeoff angle. We have ignored reflections from the free surface. When mode conversions are ignored, the free surface does not affect our results, because it simply creates a mirror image of the scattering medium above the free surface. Mode conversions at the free surface, however, would change the relative contributions of the P and S waves. As shown by the derivation of section 5.1 for a moment tensor, the final result is virtually independent of the P waves that are radiated by the source. Furthermore, the coda is saturated in S waves [*Aki and Chouet*, 1975; *Weaver*, 1982; *Papanicolaou and Ryzhik*, 1999; *Trégourès and van Tiggelen*, 2002; *Snieder*, 2002]. This means that P-to-S conversions at the free surface are not important and the effect of mode conversions by the free surface is small.

[57] Another assumption that we use is that the source radiates energy with the same radiation pattern as a source in a locally homogeneous medium. This condition is violated, for example, when the source excites strong fault zone guided waves. It is difficult to estimate the imprint of near-source heterogeneity, especially when this heterogeneity is unknown. Our theory is, however, consistent with the commonly used assumption that the radiation pattern is determined by the properties of a source in a locally homogeneous medium [*Aki and Richards*, 2002].

[58] In the derivation of expression (3) a second-order Taylor approximation of the cross correlation in the travel time perturbation has been used [*Snieder*, 2002]. This condition is satisfied when $\overline{\omega}\sigma_\tau < 1$. Physically this condition means that the source separation must be smaller than a wavelength. This is the parameter range where our technique is most useful, because the double-difference method is most effective when the event separation is comparable to a wavelength or larger.

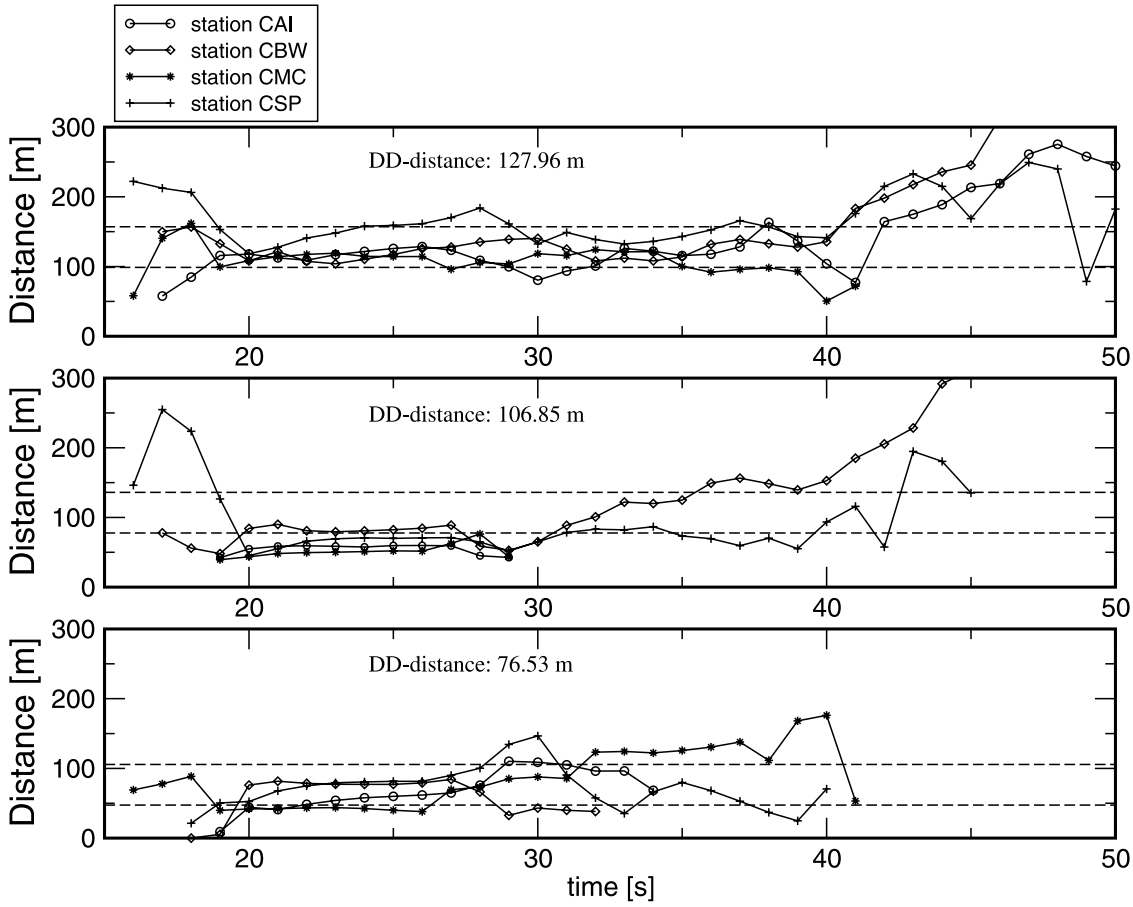

Figure 6. Calculated distances for three different event pairs: (top) pair 1, events 238295 and 242003; (middle) pair 2, events 242003 and 242020; and (bottom) pair 3 events 402093 and 402094. All three event pairs were recorded at stations CAI, CBW, CMC, and CSP. The dashed lines give the event separation obtained from the double-difference method [*Waldhauser and Ellsworth*, 2002] plus or minus one standard deviation.

[59] Our technique breaks down when the event separation is too large compared to a wavelength. When the source separation is very small compared to a wavelength, it is in practice difficult to measure the source separation accurately from the changes in the waveforms. For this reason it may be useful to frequency filter the data before applying the technique proposed here, in order to ensure that the dominant wavelength of the filtered data matches the event separation.

[60] The correlation measurement that provides the event separation can be applied to several independent time windows in the coda. The independent estimates of the source separation that are thus obtained provide a consistency check on the employed method, and also provide a basis to obtain error estimates of the source separation. The number of independent time windows that can be used depends on the noise level because the coda ceases to carry useful information when it has decayed to levels comparable to the ambient noise. It is important to apply the noise correction (55) for time intervals where the noise level is appreciable compared to the coda. Since the method relies on data from a single station only, it is possible to obtain additional independent estimates of the event separation by using waveforms from more seismological stations.

[61] In the double-difference method, the relative location of events is obtained by combining the travel time differences for different event pairs recorded at many stations. Coda wave interferometry provides a constraint on the event separation using the waveforms of one event pair only recorded at a single station. This makes it possible to use this technique to obtain a rapid estimate of the event separation. Our technique relies on the principle that the waves that constitute the coda are radiated away from the source in all possible directions. For this reason information about the direction of the event separation cannot be obtained from our method.

[62] Coda wave interferometry, as proposed here, provides additional constraints on the source separation that

Table 1. Average Distance Obtained From Coda Wave Interferometry (CWI) and Standard Deviation for Three Different Event Pairs and the Distances and Standard Deviations Obtained From the Double-Difference Method (DD)

Pair Number	Distance From CWI	Distance From DD
1	124 m ± 19 m	128 m ± 29 m
2	63 m ± 11 m	107 m ± 29 m
3	68 m ± 14 m	77 m ± 29 m

can be used in addition to the constraints imposed by using the double-difference method. When N events are located in a region of space comparable to a wavelength, our technique in principle gives $N(N-1)/2$ constraints on the distance between event pairs that can be used as a basis of a triangulation technique to determine the relative event locations [*Menke*, 1999; *Waldhauser and Ellsworth*, 2000]. Such a procedure will be most effective when it is combined with constraints obtained from the double-difference method.

Appendix A: Relative Importance of the Travel Time Change

[63] When the source location is displaced over a distance δ, the wave field u changes because of (1) the change in the arrival time, (2) a change in the geometrical spreading, and (3) a change in the energy radiated by the source or a change in the scattering amplitude. In this appendix we estimate the relative contribution of these different factors using an analysis in the frequency domain.

[64] The phase of the wave that travels over a distance $\mathbf{r}$ from a source to a scatterer is accounted for by a term $\exp(i\mathbf{k}\cdot\mathbf{r})$. When the source is displaced over a distance δ, this introduces an additional phase shift that is of the order $\exp(-ik\delta\cos\theta)$, where θ measures the angle between the takeoff direction of the ray and the source displacement. When the source displacement is much smaller than the wavelength, this phase change is given by $\exp(-ik\delta\cos\theta) \approx 1 - ik\delta\cos\theta$. Using that $k = 2\pi/\lambda$, this means that the relative change in the wave field due to the change in the travel time is to first order given by

$$(\Delta u/u)^{\text{phase}} \sim \delta/\lambda\,. \tag{A1}$$

[65] The geometric spreading is in three dimensions given by $1/r$. When the source is displaced over a distance δ, the geometrical spreading changes into $1/(r-\delta\cos\theta)$. To first order in δ, the perturbed geometrical spreading is given by $(1/r)\times(1+\delta\cos\theta/r)$, and the relative change in the wave field due to a change in geometrical spreading is given by

$$(\Delta u/u)^{\text{spreading}} \sim \delta/l\,, \tag{A2}$$

where l is the mean free path, a measure of the average distance traveled to a scatterer.

[66] A change in the source position leads to a change in the takeoff direction of each ray and also to a change in the scattering angle at each scatterer. For both cases, the change in the angle is given by $\Delta\varphi = \delta/r$. Let us assume that the source radiates with a radiation pattern $\sin(m\varphi)$ or $\cos(m\varphi)$ and that the scattering amplitude has a similar dependence on the scattering angle. In that case the relative change in the radiated or scattered waves is of the order $m\Delta\varphi$. Using that the average distance from the source to a scatterer is given by the mean free path, this gives the following contribution to the change in the waves due to a change in the source position:

$$(\Delta u/u)^{angles} \sim m\delta/l\,. \tag{A3}$$

For a point force or a moment tensor, $|m| \le 2$ [*Aki and Richards*, 2002]. This property holds as well for elastic scatterers that are much smaller than a wavelength [*Wu and Aki*, 1985]. For larger scatterers the dependence of the scattering amplitude may depend on larger values of m. In that case, however, the scattering is predominantly in the forward direction and the coda will be weak.

[67] This means that the ratio of the change in the wave due to a change in the arrival time and to other changes is given by

$$\frac{(\Delta u/u)^{\text{phase}}}{(\Delta u/u)^{\text{spreading/angles}}} \sim l/m\lambda\,. \tag{A4}$$

Note that this ratio does not depend on the source displacement δ. The change in the phase dominates when the mean free path l is much larger than a wavelength. Note that when this condition is violated, the waves are localized and clear P and S wave arrivals are not present [*van Tiggelen*, 1999]. Since a change in the phase corresponds in the time domain to a change in the arrival time, this shows that the change in the arrival time is the dominant change when the distance to the scatterers as measured by the mean free path is much larger than the dominant wavelength.

Appendix B: Noise Correction

[68] In this appendix, which follows the treatment of Douma and Snieder (submitted manuscript, 2004), we discuss the imprint of random noise on the correlation coefficient defined in equation (3). In this appendix we set the lag time equal to zero ($t_s = 0$), but the result is easily generalized to a nonzero lag time. The measured signal $u_1(t)$ consists of the signal $s_1(t)$, which would be measured in the absence of noise, and the noise $n_1(t)$. This means that

$$u_{1,2}(t) = s_{1,2}(t) + n_{1,2}(t)\,. \tag{B1}$$

For brevity we write the correlation coefficient defined in expression (3) as

$$R = \frac{\langle u_1 u_2\rangle}{\sqrt{\langle u_1^2\rangle\langle u_2^2\rangle}}\,, \tag{B2}$$

where the angle brackets denotes the time average over the employed time window. In this appendix we show how the noise-contaminated correlation coefficient given above is related to the corrected correlation coefficient defined as

$$R_{\text{corr}} = \frac{\langle s_1 s_2\rangle}{\sqrt{\langle s_1^2\rangle\langle s_2^2\rangle}}\,. \tag{B3}$$

[69] In the following, we assume that the noise time series are uncorrelated, and that the signals $s_{1,2}(t)$ are uncorrelated with the noise:

$$\langle n_1 n_2\rangle = \langle n_i s_j\rangle = 0\,. \tag{B4}$$

In a given noise realization these time averages are not exactly equal to zero, but these averages are in general much smaller than correlated averages such as $\langle n_1^2\rangle$. Using expressions (B1) and (B4), we obtain $\langle s_1 s_2\rangle = \langle u_1 u_2\rangle -$

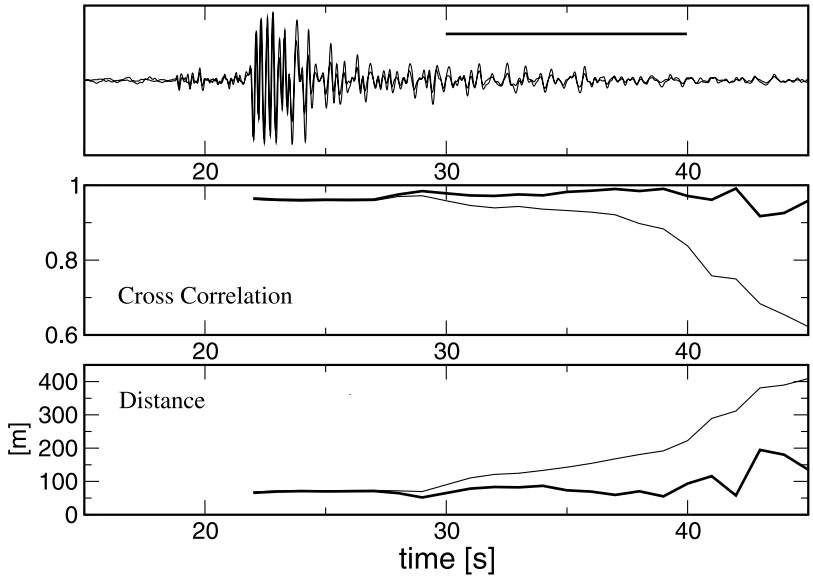

Figure B1. Uncorrected (thin line) and corrected (thick line) (middle) cross correlation and (bottom) event distance for events 242003 and 242020 recorded at station CSP. (top) Two waveforms. The horizontal bar indicates the size of the time window used to compute the cross correlation.

$\langle u_1 n_2 \rangle - \langle u_2 n_1 \rangle + \langle n_1 n_2 \rangle = \langle u_1 u_2 \rangle$. This result can be used in the numerator of (B3). Furthermore, $\langle u_1^2 \rangle = \langle s_1^2 \rangle + 2\langle s_1 n_1 \rangle + \langle n_1^2 \rangle = \langle s_1^2 \rangle + \langle n_1^2 \rangle$. In an experiment, u_1 is measured, but s_1 is unknown because the noise is unknown. The last expression can be used to eliminate $\langle s_1^2 \rangle$ from the denominator of expression (B3). Using these results and a similar expression for $\langle s_2^2 \rangle$ gives

$$R_{\text{corr}} = \frac{\langle u_1 u_2 \rangle}{\sqrt{\left(\langle u_1^2 \rangle - \langle n_1^2 \rangle\right)\left(\langle u_2^2 \rangle - \langle n_2^2 \rangle\right)}} . \qquad \text{(B5)}$$

With the definition (B2) this gives expression (55).

[70] For the derivation of the noise correction we assume that the noise is uncorrelated with the signal. For earthquake data the noise energy $\langle n_{1,2}^2 \rangle$ can be estimated from the waveforms before the first arrivals, while $\langle u_{1,2}^2 \rangle$ is computed for each time window separately. The uncorrected and corrected cross correlation for a pair of earthquake waveforms is plotted in Figure B1 (middle). The bold line corresponds to the corrected cross correlation. The uncorrected cross correlation is smaller because the noise decreases the similarity between the two waveforms. In Figure B1 (bottom) the cross correlation is converted into distance between the two sources. Again, the bold line corresponds to the distance computed from the corrected cross correlation. The distances have almost the same value for early times because the signal strength is high, and consequently, the noise level is low. As we move further in the coda, the signal-to-noise level becomes lower and the two distances deviate. The corrected distance maintains a more or less constant value further into the coda.

[71] **Acknowledgments.** Scholarships from Stichting Molengraaff Fonds, Karel Frederik Stichting and Utrecht University enabled Mark Vrijlandt to perform this research at the Colorado School of Mines. Special thanks to Alexandre Grêt for useful comments and discussions, Felix Waldhauser and Bill Ellsworth for supplying the event IDs for a useful cluster of earthquakes recorded by the Northern California Seismic Network and for supplying us with the results from the double-difference algorithm, Carlos Pacheco for helping with the synthetic experiment. We appreciate the critical comments of Ken Larner, Albena Mateeva, Greg Beroza, Haruo Sato, and Brian Zadler. This work was supported by the NSF (grant EAR-0106668).

References

Aki, K., and L. Chouet (1975), Origin of coda waves: source, attenuation, and scattering effects, *J. Geophys. Res.*, *80*, 3322–3342.

Aki, K., and P. Richards (2002), *Quantitative Seismology*, 2nd ed., Univ. Sci. Books, Sausalito, Calif.

Astiz, L., and P. Shearer (2000), Earthquake locations in the inner Continental Borderland, offshore southern California, *Bull. Seismol. Soc. Am.*, *90*, 425–449.

Bokelmann, G., and H. Harhes (2000), Evidence for temporal variation of seismic velocity within the upper continental crust, *J. Geophys. Res.*, *105*, 23,879–23,894.

Deichmann, N., and M. Garcia-Fernandez (1992), Rupture geometry from high-precision relative hypocenter location of microearthquake clusters, *Geophys. J. Int.*, *110*, 501–517.

Frémont, M., and S. Malone (1987), High precision relative locations of earthquakes at Mount St. Helens, Washington, *J. Geophys. Res.*, *92*, 10,223–10,236.

Fuis, G., T. Ryberg, W. Lutter, and P. Ehlig (2001), Seismic mapping of shallow fault zones in the San Gabriel Mountains from the Los Angeles region seismic experiment, southern California, *J. Geophys. Res.*, *106*, 6549–6568.

Got, J., J. Fréchet, and F. Klein (1994), Deep fault plane geometry inferred from multiplet relative location beneath the south flank of Kilauea, *J. Geophys. Res.*, *99*, 15,375–15,386.

Ito, A. (1985), High-resolution relative hypocenters of similar earthquakes by cross-spectal analysis method, *J. Phys. Earth*, *33*, 279–294.

Lay, T., and T. Wallace (1995), *Modern Global Seismology*, Springer, New York.

Lees, J. (1998), Multiplet analysis at Coso geothermal, *Bull. Seismol. Soc. Am.*, *88*, 1127–1143.

Maxwell, S., and T. Urbancic (2001), The role of passive microseismic monitoring in the instrumented oil field, *Leading Edge*, *20*(6), 636–639.

Menke, W. (1999), Using waveform similarity to constrain earthquake locations, *Bull. Seismol. Soc. Am.*, *89*, 1143–1146.

Nadeau, R., and T. McEvilly (1997), Seismological studies at Parkfield V: Characteristic microearthquake sequences as fault-zone drilling targets, *Bull. Seismol. Soc. Am.*, *87*, 1463–1472.

Papanicolaou, G., and L. Ryzhik (1999), *Waves and Transport*, *IAS/Park City Math. Ser.*, vol. 5, pp. 307–382, Am. Math. Soc., Providence, R. I.

Pavlis, G. (1992), Appraising relative eartquake location errors, *Bull. Seism. Soc. Am.*, *82*, 836–859.

Poupinet, G., W. Ellsworth, and J. Fréchet (1984), Monitoring velocity variations in the crust using earthquake doublets: An application to the Calaveras Fault, California, *J. Geophys. Res.*, *89*, 5719–5731.

Scherbaum, F., and J. Wendler (1986), Cross spectral analysis of Swabian Jura (SW Germany) three-component earthquake recordings, *J. Geophys. Res.*, *60*, 157–166.

Shapiro, S., E. Rothert, V. Rath, and Rindschwentner (2002), Characterization of fluid transport properties of reservoirs using induced microseismicity, *Geophysics*, *67*, 212–220.

Shearer, P. (1997), Improving local earthquake locations using the L_1 norm and waveform cross correlation: Application to the Whittier Narrows California aftershock sequence, *J. Geophys. Res.*, *102*, 8269–8283.

Snieder, R. (1999), Imaging and averaging in complex media, in *Diffuse Waves in Complex Media*, edited by J. Fouque, pp. 405–454, Springer, New York.

Snieder, R. (2002), Coda wave interferometry and the equilibration of energy in elastic media, *Phys. Rev. E*, *66*, 046615.

Snieder, R. (2004a), Extracting the Green's function from the correlation of coda waves: A derivation based on stationary phase, *Phys. Rev. E*, *69*, 046610.

Snieder, R. (2004b), Coda wave interferometry, in *2004 McGraw-Hill Yearbook of Science and Technology*, pp. 54–56, McGraw-Hill, New York.

Snieder, R., and M. Hagerty (2004), Monitoring change in volcanic interiors using coda wave interferometry: Application to Arenal Volcano, Costa Rica, *Geophys. Res. Lett.*, *31*, L09608, doi:10.1029/2004GL019670.

Snieder, R., A. Grêt, H. Douma, and J. Scales (2002), Coda wave interferometry for estimating nonlinear behavior in seismic velocity, *Science*, *295*, 2253–2255.

Trégourès, N., and B. van Tiggelen (2002), Generalized diffusion equation for multiple scattered elastic waves, *Waves Random Media*, *12*, 21–38.

VanDecar, J., and R. Crosson (1990), Determination of teleseismic relative phase arrival times using multi-channel cross-correlation and least-squares, *Bull. Seismol. Soc. Am.*, *80*, 150–169.

van Tiggelen, B. A. (1999), Localization of waves, in *Diffuse Waves in Complex Media*, edited by J. Fouque, pp. 1–60, Springer, New York.

Waldhauser, F., and W. Ellsworth (2000), A double-difference earthquake location algorithm: Method and application to the northern Hayward fault, California, *Bull. Seismol. Soc. Am.*, *90*, 1353–1368.

Waldhauser, F., and W. L. Ellsworth (2002), Fault structure and mechanics of the Hayward Fault, California, from double-difference earthquake locations, *J. Geophys. Res.*, *107*(B3), 2054, doi:10.1029/2000JB000084.

Weaver, R. (1982), On diffuse waves in solid media, *J. Acoust. Soc. Am.*, *71*, 1608–1609.

Wu, R. S., and K. Aki (1985), Elastic wave scattering by a random medium and the small-scale inhomogeneities in the lithosphere, *J. Geophys. Res.*, *90*, 10,261–10,273.

R. Snieder and M. Vrijlandt, Department of Geophysics and Center for Wave Phenomena, Colorado School of Mines, Golden, CO 80401, USA. (rsnieder@mines.edu)